Transfer of spectral weight in spectroscopies of correlated electron systems

M. J. Rozenberg*
Laboratoire de Physique Théorique, Ecole Normale Supérieure, 24 rue Lhomond, 75231 Paris Cedex 05, France

G. Kotliar and H. Kajueter
Serin Physics Laboratory, Rutgers University, Piscataway, New Jersey 08855-0849
(Received 2 October 1995; revised manuscript received 23 February 1996)

We study the transfer of spectral weight in the photoemission and optical spectra of strongly correlated electron systems. Within the local impurity self-consistent approximation, that becomes exact in the limit of large lattice coordination, we consider and compare two models of correlated electrons, the Hubbard model and the periodic Anderson model. The results are discussed in regard to recent experiments. In the Hubbard model, we predict an anomalous enhancement optical spectral weight as a function of temperature in the correlated metallic state which is in qualitative agreement with optical measurements in V_2O_3. We argue that anomalies observed in the spectroscopy of the metal are connected to the proximity to a crossover region in the phase diagram of the model. In the insulating phase, we obtain excellent agreement with the experimental data, and present a detailed discussion on the role of magnetic frustration by studying the k-resolved single-particle spectra. The results for the periodic Anderson model are discussed in connection to recent experimental data of the Kondo insulators $Ce_3Bi_4Pt_3$ and FeSi. The model can successfully explain the thermal filling of the optical gap and the corresponding changes in the photoemission density of states. The temperature dependence of the optical sum rule is obtained, and its relevance to the interpretation of the experimental data discussed. Finally, we argue that the large scattering rate measured in Kondo insulators cannot be described by the periodic Anderson model. [S0163-1829(96)05536-1]

I. INTRODUCTION

Interest in the distribution of spectral weight in the optical conductivity of correlated electron systems has been revived by the improvement of the quality of the experimental data in various systems.[1–3] The traditional methods used in the strong correlation problem—exact diagonalization of small clusters,[4] slave boson approaches,[5] and perturbative calculations—have not been very successful in describing the interesting transfer of optical weight which takes place as a function of temperature in the strong correlation regime.

Recently, much progress has been achieved by mapping lattice models into impurity models embedded in an effective medium. This technique, the local impurity self-consistent approximation (LISA),[6] is a dynamical mean-field theory that becomes exact in the limit of a large number of spatial dimensions.[7] For instance, the Hubbard and Anderson lattice models can both both mapped onto the Anderson impurity model subject to different self-consistency conditions for the conduction-electron bath.[8,9] These resulting self-consistent impurity problems can be analyzed by a variety of numerical techniques.[10–19]

In this paper we apply this approach to a study of the optical conductivity in regard to recent experiments in V_2O_3, $Ce_3Bi_4Pt_3$, and FeSi. We assume that the *low-energy* optical properties of V_2O_3 can be modeled by a one-band Hubbard model, while $Ce_3Bi_4Pt_3$ and FeSi are described by a periodic Anderson model.[20] Due to the localized character of the orbitals that are expected to play relevant roles in the low-frequency response, the modeling of the experimental systems requires a large value of the Coulomb repulsion U.

Our main goal in this work is to demonstrate that simplified models of strongly interacting systems treated with the LISA may account for some of the main qualitative features that are observed experimentally in the aforementioned strongly correlated electron compounds. We have intentionally chosen to consider both the Hubbard and periodic Anderson models within the same work in order to emphasize the interesting connections in the behavior of these seemingly very different models. In this regard, one of the most insightful results is the notable temperature dependence that affects the optical response of the models. The reason for this important effect (which is experimentally observed) is in the competition between the temperature and a *dynamically generated low-energy scale*, namely, the ''Kondo'' temperature of the associated single-impurity model, which is obtained upon the mapping of *either* model Hamiltonian.

The paper is organized as follows: in Sec. II we summarize the mean-field equations for the model Hamiltonians and the expressions for the calculation of the optical conductivity and the optical sum rule. In Sec. III we present an intuitive pedagogical discussion of the physical content of the solution of the model Hamiltonians in the large dimensional limit. Section IV is dedicated to a thorough discussion of the optical conductivity results. We discuss the effects on the spectral functions of the introduction of magnetic frustration in the Hubbard model which appears as an important ingredient in the physics of the V_2O_3 compound. Also, we consider the effects of temperature and disorder on the optical response of the model Hamiltonians. The calculations are carried out using exact diagonalization (ED) and iterated perturbation theory (IPT) techniques, and the theoretical results are discussed in regard of the experimental ones obtained on various systems. Part of the theoretical results in Sec. IV

were announced in a recent letter.[21]

The optical conductivity of the Anderson and Hubbard models were considered previously by Jarrell and co-workers using the quantum Monte Carlo (QMC) and maximum entropy methods.[14,22–25] However, such techniques cannot be applied to the rather high values of the interaction and low temperatures which are relevant for the experimental regime. For this reason we extensively use the IPT method, that allows us to access physically interesting regimes which are outside the applicability of the QMC method. We also use the ED technique which, like the QMC, is an exact method, to confirm that the results presented are genuine features of the model solutions in the limit of infinite dimensions, and not artifacts of the IPT.

The conclusions are presented in Sec. V, and we finally note that our ED approach to the solution of correlated models in large dimensions is based on the use of continuous fractions. The Appendix describes an algorithm to convert the sum of two given continued fractions into a continued fraction which we use to extend the ED method to the models we treat in this paper.

II. METHODOLOGY

A. Mean-field equations

As model Hamiltonians we consider the Hubbard model and the periodic Anderson model (PAM):

$$H_H=-\sum_{<i,j>}(t_{ij}+\mu)c_{i\sigma}^{\dagger}c_{j\sigma}+\sum_i U(n_{i\uparrow}-\tfrac{1}{2})(n_{i\downarrow}-\tfrac{1}{2}), \tag{1}$$

$$H_{\mathrm{PA}}=\sum_k(\epsilon_k-\mu)c_{k\sigma}^{\dagger}c_{k\sigma}+\sum_i(\epsilon_d^o-\mu)d_{i\sigma}^{\dagger}d_{i\sigma} +\sum_i V(d_{i\sigma}^{\dagger}c_{i\sigma}+\mathrm{H.c.})+\sum_i U(n_{di\uparrow}-\tfrac{1}{2})(n_{di\downarrow}-\tfrac{1}{2}), \tag{2}$$

where summation over repeated spin indices is assumed. μ is the chemical potential, and t_{ij} is the hopping amplitude between the conduction-electron sites, which in the PAM results in the band ϵ_k. The $d^{\dagger}$ and d operators create and destroy electrons on localized orbital with energy ϵ_d^o. V is the hybridization amplitude between c and d sites, which also appear in the literature as d and f sites, respectively.

The derivation has been given in detail elsewhere,[8,9] and in particular in Ref. 6. So we choose to present only the final expressions here. The resulting local effective action reads

$$S_{\mathrm{local}}=-\int_0^{\beta}d\tau\int_0^{\beta}d\tau'\,\psi_{\sigma}^{\dagger}(\tau)\mathcal{G}_0^{-1}(\tau-\tau')\psi_{\sigma}(\tau') +U\int_0^{\beta}d\tau[n_{\uparrow}(\tau)-\tfrac{1}{2}][n_{\downarrow}(\tau)-\tfrac{1}{2}] \tag{3}$$

where $\psi_{\sigma}^{\dagger}$ and ψ_{σ} correspond to a particular site, and denote $c_{\sigma}^{\dagger}$ and c_{σ} in the Hubbard model, and $\{c_{\sigma}^{\dagger},d_{\sigma}^{\dagger}\}$ and $\{c_{\sigma},d_{\sigma}\}$ in the PAM case. n_{σ} corresponds to $n_{c\sigma}$ and $n_{d\sigma}$, respectively. Also note that Eq. (3) defines the associated impurity problem, with $\psi_{\sigma}^{\dagger}$ and ψ_{σ} being the operators at the impurity site while the information on the hybridization with the environment is implicitly contained in $\mathcal{G}_0^{-1}$. Requiring that

$$G_{\mathrm{local}}(\omega)=\Sigma_k G(k,\omega), \tag{4}$$

we obtain, as a self-consistency condition,

$$\mathcal{G}_0^{-1}(\omega)=\omega+\mu-t^2\widetilde{G}(\omega), \tag{5}$$

for the Hubbard model, and

$$[\mathcal{G}_0^{-1}]_{cc}(\omega)=\omega+\mu-t^2[\widetilde{G}]_{cc}(\omega) \tag{6}$$

with $\mathcal{G}_0$ explicitly given by

$$\mathcal{G}_0^{-1}(i\omega)=\begin{pmatrix} i\omega-t^2[\widetilde{G}]_{cc}(i\omega) & V \\ V & i\omega \end{pmatrix} \tag{7}$$

for the PAM. In both cases, $\widetilde{G}$ is the ''cavity'' Green function which has the information of the response of the lattice.

We consider a symmetric case with $\mu=0$ and $\epsilon_d^o=0$. Moreover, we assume a semicircular bare density of states for the conduction electrons, $\rho^o(\epsilon)=\Sigma_k\delta(\epsilon-\epsilon_k)/N_{\mathrm{sites}}=(2/\pi D)\sqrt{1-(\epsilon/D)^2}$, with the half-bandwidth $D=2t$. This density of states can be realized in a Bethe lattice and also on a fully connected fully frustrated version of the model.[13,15] In this case the ''cavity'' Green function simply becomes $\widetilde{G}=G$. In the following we set the half-bandwidth $D=1$. We use an exact diagonalization algorithm (ED) (Refs. 17 and 18) and an extension of the second-order iterative perturbation theory (IPT) to solve the associated impurity problem.[13] We have checked that IPT and ED methods are in good agreement for all values of the model parameters. This results from the property of IPT to capture the atomic limit exactly in the symmetric case.[13] We extensively use IPT on the real axis to scan through parameter space. A detailed comparison will be presented elsewhere.

B. Optical conductivity

The optical conductivity of a given system is defined by

$$\sigma(\omega)=\frac{1}{\mathcal{V}\omega}\,\mathrm{Im}\int_0^{\infty}\langle[\mathcal{J}(t),\mathcal{J}(0)]\rangle e^{i\omega t}dt \tag{8}$$

where $\mathcal{V}$ is the volume, $\mathcal{J}$ is the current operator, and $\langle\,\rangle$ indicates an average over a finite-temperature ensemble or over the ground state at zero temperature. In general, $\sigma(\omega)$ obeys a version of the f-sum rule,[26,27]

$$\int_0^{\infty}\sigma(\omega)d\omega=\frac{\pi}{\mathcal{V}}\mathrm{Im}\langle[P,\mathcal{J}]\rangle \tag{9}$$

where P is a polarization operator obeying $\partial P/\partial t=\mathcal{J}$.

In a model which includes *all electrons and all bands*, the current operator $\mathcal{J}$ is given by

$$\mathcal{J}=\frac{e}{m}\sum_i p_i\delta(r-r_i), \tag{10}$$

where p_i is the momentum and r_i the position of the ith electron, and e and m denote its charge and bare mass. P is given by

$$P = e\sum_i r_i \delta(r - r_i). \tag{11}$$

Thus $1/\mathcal{V}\langle[P,\mathcal{J}]\rangle = ine^2/m$, where n is the density of electrons, and the sum rule becomes

$$\int_0^\infty \sigma(\omega)d\omega = \pi\frac{ne^2}{m}. \tag{12}$$

This result is clearly temperature independent, and does not depend on the strength of the interactions.

When dealing with strongly correlated electron systems, in a frequency range where few of the bands are believed to be important, it is customary to work with an effective model with one or two bands, such as the Hubbard or periodic Anderson model. The current operator is thus projected onto the low-energy sector, and is expressed in terms of creation and destruction operators of the relevant bands (i.e., $\mathcal{J} = i[eat/\hbar\nu)\Sigma_i(c^\dagger_{i+\delta}c_i - c^\dagger_i c_{i+\delta})]$ for the Hubbard and Anderson models with nearest-neighbor hopping). In this case the expectation value $\langle[P,\mathcal{J}]\rangle$ is no longer $\sim ne^2/m$, but becomes

$$i(e^2/\hbar\nu)\sum_k \langle c_k^+ c_k\rangle \frac{\partial^2\epsilon_k}{K_x^2},$$

which is proportional to the expectation value of the kinetic energy $\langle K\rangle$ of the conduction electrons in the case of NN hopping.[26,28] In general, $\langle K\rangle$ depends on the temperature and strength of interactions; therefore, for these few-band models, the optical weight sum rule will depend on them as well. If the projection onto a few-band model is valid, this result also implicitly indicates that a portion of the optical spectral weight (the weight not exhausted by $\langle K\rangle$) is transferred to much higher energies; that is, to bands that were excluded by the projection to low energies.

In this paper we do not address the question of the validity of the low-energy projection onto a few-band model. Instead we focus on the consequences of this assumption on the redistribution of the optical weight within a mean-field theory that is exact in the limit of large dimensions. Our main conclusion is that there is a considerable temperature dependence of the integrated spectral weight appearing in the sum rule.

In infinite dimensions, $\sigma(\omega)$ can be expressed in terms of the one-particle spectrum of the current-carrying electrons:[29,23]

$$\sigma(\omega) = \frac{1}{\omega}\frac{2e^2t^2a^2}{\nu\hbar^2}\int_{-\infty}^{\infty} d\epsilon\,\rho^o(\epsilon)\int_{-\infty}^{\infty}\frac{d\omega'}{2\pi}A_\epsilon(\omega')A_\epsilon(\omega'+\omega) \times[n_f(\omega') - n_f(\omega'+\omega)], \tag{13}$$

with $A_\epsilon(\omega) = -2\,\mathrm{Im}[G_k(\omega)]$ being the spectral representation of the Green function of the lattice conduction electrons, a the lattice constant, and ν the volume of the unit cell.

As we anticipated, the kinetic energy is related to the conductivity by the sum rule

$$\int_0^\infty \sigma(\omega)d\omega = -\frac{\pi e^2 a^2}{2d\hbar^2\nu}\langle K\rangle = \frac{\omega_P^2}{8\pi}. \tag{14}$$

An important result, which will be demonstrated later on, is the notable dependence of the plasma frequency ω_P on temperature. This feature will be seen to emerge because correlation effects generate small energy scales (e.g., the ''Kondo temperature'' of the associated impurity). It is the competition between the small scales and the temperature that gives rise to an unusual temperature dependence to the integrated optical spectral weight.

At $T=0$, the optical conductivity of a metallic correlated electron system can be parametrized by[27]

$$\sigma(\omega) = \frac{\omega_P^{*2}}{4\pi}\delta(\omega) + \sigma_{\mathrm{reg}}(\omega), \tag{15}$$

where the coefficient in front of the δ function is the Drude weight, and ω_P^* is the renormalized plasma frequency. In the presence of disorder, $\delta(\omega)$ is replaced by a lorentzian of width Γ.

Evaluating Eq. (13) at $T=0$, one finds in mean-field theory that

$$\frac{\omega_P^{*2}}{4\pi} = \frac{2\pi e^2}{\hbar^2\nu}Z\sum_k\left(\frac{\partial\epsilon_k}{\partial k_x}\right)^2\delta(\epsilon_k), \tag{16}$$

where Z is the quasiparticle weight. For the Hubbard model in infinite dimensions the expression above further simplifies, and it depends only on the density of states

$$\frac{\omega_P^{*2}}{4\pi} = \frac{4\pi t^2e^2a^2}{\hbar^2\nu}Z\rho^o(0). \tag{17}$$

III. PHYSICAL CONTENT OF THE MEAN-FIELD THEORY

In the next two subsections we shall discuss in a pedagogical and intuitive manner the physical content of the Hubbard and periodic Anderson models within the dynamical mean-field theory. The discussion is based and resumes recent results,[14–16,21–25] and also serves as on introduction for the results that will be presented in detail in Sec. IV.

A. Hubbard model

The solution of the mean-field equations shows that at low temperatures the model has a metal-insulator transition (Mott-Hubbard transition) at an intermediate value of the interaction $U_c \approx 3D$.[14–16] The metallic side is characterized by a density of states (DOS) with a three-peak structure: a central feature at the Fermi energy that narrows as one moves toward U_c from below, and two broader incoherent features that develop at $\pm U/2$, namely, the lower and upper Hubbard bands. They have a width $\approx 2D$, and their spectral weight increases as the transition is approached. The insulator side, for $U > U_c$, presents only these last two high-frequency features, which are separated by an excitation gap of size $\Delta \approx U - 2D$. The different structures of the DOS (Fig. 1) give rise to very different optical responses.

Let us first consider the insulator, which is simpler. In this case, optical transitions are possible from the lower to the upper Hubbard bands. We therefore expect the optical spectrum that results from the convolution (13) to display a single broad feature that extends approximately from

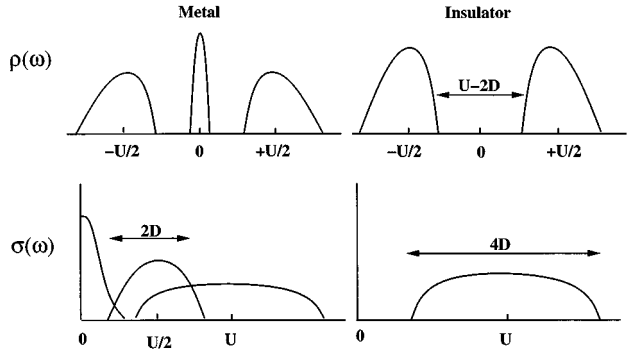

FIG. 1. Schematic DOS for the Hubbard model (half-filling) and their corresponding optical spectra for the metallic and insulator solutions. The width of the incoherent peaks in the DOS is $\approx 2D$, and the one of central peak in the metal is $\approx ZD \equiv \epsilon_F^*$

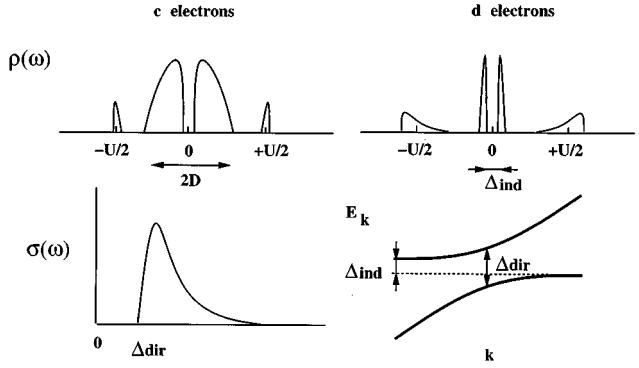

FIG. 2. Schematic DOS (half-filling) for c and d electrons in the PAM (top). The corresponding schematic optical spectra at $T=0$ (bottom left) and the schematic band structure with the direct and indirect gaps (bottom right).

$U-2D$ to $U+2D$ (Fig. 1). A negligible temperature dependence of the spectra is expected, as long as $T \ll \Delta$. On the other hand, in the metallic case, the low-temperature optical spectrum displays various contributions: (i) A narrow low-frequency peak that is due to transitions within the quasiparticle resonance; at the $T=0$ limit this peak becomes a δ function, and is the Drude part of the optical response. (ii) At frequencies of order $U/2$ an incoherent feature of width $\sim 2D$ emerges due to transitions between the Hubbard bands and the central resonance. (iii) A last contribution at frequency $\sim U$ appears due to transitions between the Hubbard bands. This is a broad feature of width $\sim 4D$. Therefore, we expect an optical spectrum which is schematically drawn in Fig. 1. It is important to realize that, unlike the insulator, a notable temperature dependence of the spectra is to be expected. There is a low-energy scale $T_{\rm coh}$ that corresponds to the temperature below which coherent quasiparticle excitations are sustained. It roughly corresponds to the width of the resonance at the Fermi energy $\epsilon_F^* \equiv ZD$. As T is then increased and becomes comparable to $T_{\rm coh}$, the quasiparticles are destroyed, and as a consequence, the contributions to the optical spectra associated with them, (i) and (ii) rapidly decrease.

It should be clear that in our previous discussion we assumed that the system does not order magnetically, as paramagnetic solutions were considered. This situation can in fact be realized by the introduction of disorder (e.g., a random distribution of t_{ij}) or next-nearest-neighbor hopping, and avoids the artificial nesting property of the bipartite lattice.[15,16]

B. Periodic Anderson model

We now present a schematic discussion of the periodic Anderson model solution. In this case there are two different types of electrons; c electrons, which form a band, and d electrons with localized orbitals. In the noninteracting particle-hole symmetric case, the hybridization amplitude V opens a gap in the c-electron density of states $\Delta_{\rm ind} \sim V^2/D$. On the other hand, the original δ-function peak of the localized d electrons broadens by hybridizing with the conduction electrons and also opens a gap $\Delta_{\rm ind}$.

When the effect of the interaction term is considered, as the local repulsive U is increased, one finds that for low frequencies the noninteracting picture which was just described still holds; though with the bare hybridization V being renormalized to a smaller value V^*. Thus we say we have a hybridization band insulator with the hybridization amplitude renormalized by interactions. This can also be interpreted by considering that the interacting d electrons form a band of ''Kondo-like'' quasiparticles, that allows us to define a coherence temperature T^* similar to the $T_{\rm coh}$ introduced above. This coherent band further opens a gap due to the periodicity of the lattice. This is the well-known scenario that is borne out from slave-boson mean-field theory and variational calculations.[30] On the other hand, the present dynamical mean-field theory also captures the high-energy part of the d-electron density of states that develops incoherent satellite peaks at frequencies $\pm U/2$ with a spectral weight that is transferred from low frequencies. Consequently, the c-electron density of states is mainly made of a central broadband of half-width $D=2t$ and a gap at the center that narrows as $V \to V^*$. Also, it develops some small high-frequency structures, that result from the hybridization with the d electrons. In Fig. 2 we schematically present the density of states for the c and d electrons. As in the Hubbard model, we assume the absence of magnetic long-range order (MLRO). For a study of the magnetic phase of the Anderson model see Ref. 31.

Since the d sites are localized orbitals, only the c electrons contribute to the optical response of this system. At $T=0$, following the previous interpretation in terms of a renormalized noninteracting hybridization band insulator and Eq. (13), we expect to find an optical conductivity spectra with a gap $\Delta_{\rm dir}$, which decreases as the interaction is increased. We also expect that $\Delta_{\rm ind} \ll \Delta_{\rm dir}$, as the first corresponds to the *indirect* gap from the density of states $\Delta_{\rm ind} \sim V^{*2}/D$, while the second is the *direct* gap $\Delta_{\rm dir} \sim V^*$ that is defined as the minimum energy for interband transitions at a given k (see Fig. 2). We do not expect any other important contributions to the optical response since, as we argued above, the incoherent high-frequency structures of the c-electron density of states do not carry much spectral weight. In Fig. 2 we schematically present the optical response at $T=0$.

As the temperature is increased, the gap in the optical conductivity becomes gradually filled. At high temperatures a simple picture of electrons scattering off local moments emerges. The crossover between these two regimes, would naively be expected to occur at a temperature of the order of Δ_{ind}.

Thus we note that in the Hubbard and periodic Anderson models the destruction of a coherent quasiparticle state that sets the low-energy scale of the system has rather *opposite* effects in the optical response. In the first case, the correlated metallic state is destroyed as T becomes of the order of the renormalized Fermi energy, and the Drude part of the optical response is transferred to higher energies as the insulating state sets in. In the second case, however, the destruction of the coherent excitations is accompanied by the thermal closing of the gap in the density of states that turns the system metallic. As a consequence, the gap of the optical response is filled with spectral weight from higher energies to become a broad Drude-like feature.

IV. RESULTS

A. Hubbard model

In this section we discuss the theoretical results for the model in regard of recent experimental data on the V_2O_3 system. To facilitate our subsequent theoretical discussion, we shall first briefly present some of the optical conductivity measurements recently reported for this compound. We shall use the experimental results in order to extract the input parameters for our model calculation. We shall not attempt to give a formal justification for these parameters, as this lies beyond the scope of our present approach, but rather assume them as a phenomenological fit that allows our model calculations to reproduce the unusual features observed in the behavior of the optical spectra qualitatively.

1. Experimental spectra of V_2O_3

Vanadium oxide has three t_{2g} orbitals per V atom which are filled with two electrons. From the work of Castellani, Natoli, and Ranninger,[32] two electrons (one per V) are engaged in a strong cation-cation bond, leaving the remaining two in a twofold-degenerate e_g band. The single-band Hubbard model ignores the degeneracy of the band, which is crucial for understanding the magnetic structure,[32] but captures the important interplay of the electron-electron interactions and the kinetic energy. This delicate interplay of itinerancy and localization is responsible for many of the anomalous properties of this compound, which are correctly predicted by this simplified model.[21] The localized character of the orbitals that are relevant for the present low frequency discussion is also borne out of local-density-approximation calculations that give a rather small bandwidth of ~ 0.5 eV.[33]

Experimentally one can vary the parameters U and D, by introducing O and V vacancies or by applying pressure or chemical substitution of the cation. We can use experimental data to extract approximate parameters to be used as input to our model. In particular, from the experimental optical conductivity data in the insulating phase, a rather accurate determination can be made because, as is apparent from the spectra, the low-frequency contribution is mainly due to a single peak.[1] In regard to our schematic discussion of the Sec. III, the position of the maximum should approximately correspond to the parameter U that corresponds to transitions from the lower to the upper Hubbard band. Also, according to the picture of Sec. III, the total width of the peak should be $\sim 4D$, which is twice the width of the Hubbard bands. Therefore, we can approximately estimate the parameter D as the distance from position of the peak maximum to the frequency where the feature decreased to half its height (see Fig. 3).

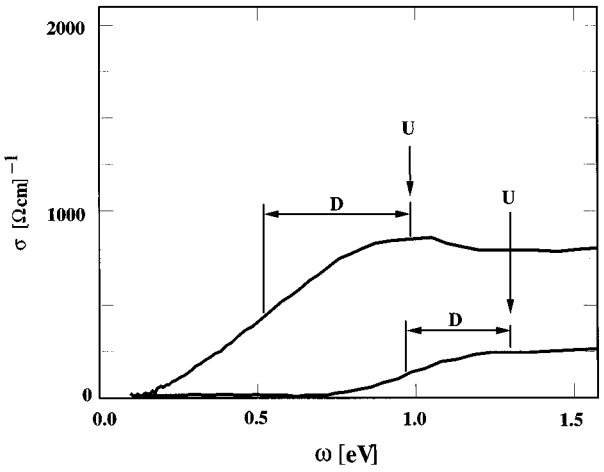

FIG. 3. The experimental $\sigma(\omega)$ of insulating $V_{2-y}O_3$ with $y=0.013$ at 10 K (upper) and $y=0$ at 70 K (lower). We indicate in the spectra the position of the maxima and their width from which the parameters U and D for the model calculations are extracted (from Ref. 35).

The parameters from the metallic optical conductivity spectra are not so easily extracted. However, we can still obtain a rather precise determination by considering the *difference spectra* between the data at 170 and 300 K (see the inset of Fig. 4).

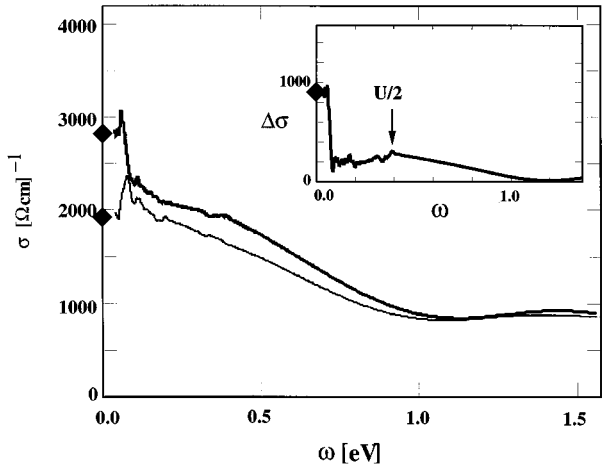

FIG. 4. The experimental $\sigma(\omega)$ of metallic V_2O_3 at $T=170$ K (upper) and $T=300$ K (lower). The inset contains the difference of the two spectra $\Delta\sigma(\omega)=\sigma_{170\,\mathrm{K}}(\omega)-\sigma_{300\,\mathrm{K}}(\omega)$. Diamonds indicate the measured dc conductivity σ_{dc} (from Ref. 21).

TABLE I. Experimental parameters for the model.

Phase	Parameter			
	D (eV)	U (eV)	Δ (eV)	$\omega_P^2/8\pi$ (eV/Ω cm)
Ins. ($y=0$)	0.33 ± 0.05	1.3 ± 0.05	0.64 ± 0.05	170 ± 20
Ins. ($y=0.013$)	0.46 ± 0.05	0.98 ± 0.05	0.08 ± 0.05	800 ± 50
Metal (170 K)	0.4 ± 0.1	0.8 ± 0.1		1700 ± 300

As we shall discuss below in detail, the feature that appears in the difference spectra at a frequency ≈ 0.4 eV can be associated with the parameter $U/2$ (this statement will be justified *a posteriori* by the results of Sec. IV A 3). It is also intuitively suggested by the schematic discussion of Sec. III that this feature corresponds to the enhancement of transitions from the lower Hubbard band to the central resonance at the Fermi level, and from the resonance to the upper Hubbard band which are at a distance $\sim U/2$. The value for the parameter $D\approx 0.4$ eV in the metallic phase was determined by noting that (i) *a priori* there is no reason to expect that it should be much different than in the insulating phase (unlike the parameter U which could be modified by screening); (ii) it is consistent with the recent LDA calculation that gives a half-width of ≈ 0.5 eV for the narrow bands at the Fermi level;[33] (iii) despite the lack of very good experimental resolution, the value is consistent with both the optical data that we reproduce in Fig. 4 and photoemission experiments;[34] and (iv) as will be shown later in the paper, this estimated value will allow us to gather in a single semiquantitative consistent picture the optical conductivity results with the V_2O_3 phase diagram[21] and experimental results for the slope of the specific heat. The extracted parameters, along with the values for the size of the optical gap (in the insulators), and the total optical spectral weight are summarized in Table I.

2. Insulating state

We now turn to optical conductivity results. The experimental optical spectrum of the insulator was reproduced in Fig. 3.[35] It is characterized by an excitation gap at low energies, followed by an incoherent feature that corresponds to charge excitations of mainly vanadium character.[1] These data are to be compared with the model results of Fig. 5. The overall shape of the spectrum is found to be in very good agreement with the experimental results for the pure V_2O_3 sample. We display the optical spectra results from both IPT and ED methods. The data show very good agreement between these two methods. The peak structure in the ED data is due to the finite number of poles that result from the finite size of the clusters that can be considered in practice.

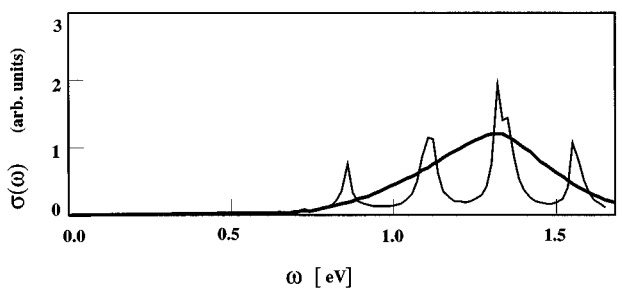

FIG. 5. The model $\sigma(\omega)$ for the insulating solution results at $U=4D$ and $T=0$ from ED (thin) and IPT (bold).

In Fig. 6 we display the results for the size of gaps Δ, which are in excellent agreement with the experimental results indicated by black squares.[35] It is interesting to note that the results of Fig. 6, shown for various degrees of magnetic frustration (c.f. Sec. IV A 4), indicate that in V_2O_3 frustration plays an important role. The experimental system seems to be closer to the limit of strong frustration, which is consistent with neutron-scattering results that indicate different signs for the magnetic interactions between different neighboring sites.[36]

Another interesting point is the fact that the gap obtained in the model optical spectra and the one obtained from the position of the poles in the single-particle spectra coincide (Figs. 5 and 6). We therefore conclude that in this model the direct and indirect gaps are very close (which justifies *a posteriori* that Δ is measured from the lowest pole of the local Green function). This result, already predicted in Ref. 21, was experimentally confirmed by accurate recent photoemission study of V_2O_3.[37] This follows from the fact that the imaginary part of the self-energy is very large wherever the electron density of states is non zero in the insulating solution (see Fig. 7). This is nothing but a direct consequence of the complete incoherent character of the upper and lower Hubbard bands. They describe a completely incoherent propagation, and one should not think of them as usual metallic bands ''shifted'' by the interaction U. This is an interesting result, as we note that from the discussion in Sec. III,

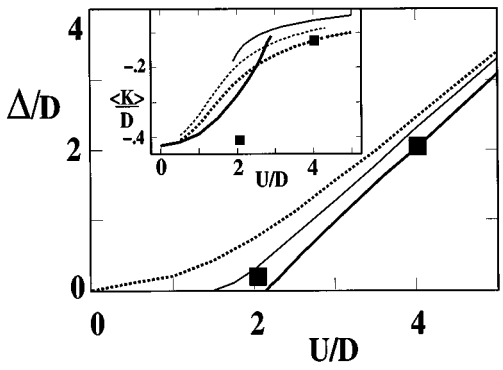

FIG. 6. The gap Δ vs U for the antiferromagnetic, partially frustrated, and paramagnetic insulators (dotted, thin, and bold). Δ is twice the energy of the lowest pole from the ED Green function. The data are for $n_s\rightarrow\infty$ from clusters of three, five, and seven sites assuming $1/n_s$ scaling behavior. Black squares show the experimental gap for $V_{2-y}O_3$ with $y=0.0$ and 0.013. Inset: $\langle K\rangle$ versus V for the AFI (bold-dotted), PI (thin) PM (bold), and partially frustrated model (thin-dotted). Black squares show the experimental results.

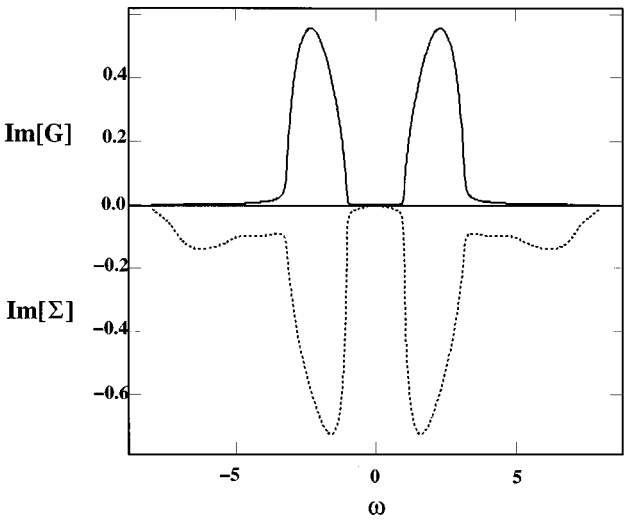

FIG. 7. Im$[G(\omega)]$ and Im$[\Sigma(\omega)]$ for $U=4$ from IPT. Note that Im$[\Sigma(\omega)]$ is large when Im$[G(\omega)]$ is nonzero, indicating the incoherent character of the particle excitations.

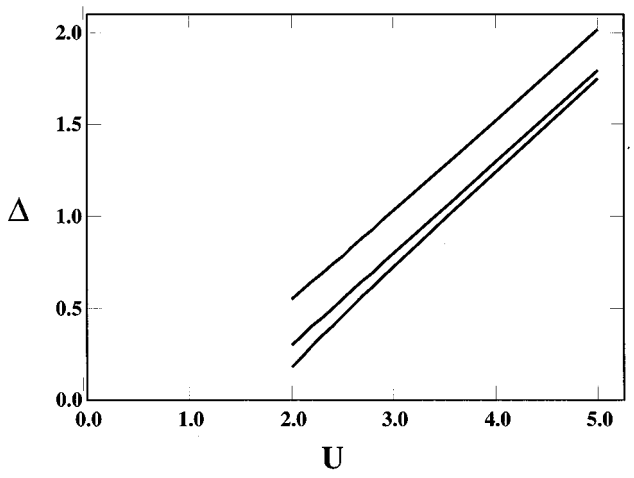

FIG. 8. The gap Δ vs the interaction U in the paramagnetic insulator. Δ is twice the energy of the lowest pole from the ED Green function. The data are from clusters of three, five, and seven sites (top to bottom).

in the unfrustrated case, one would have expected the direct gap to be larger that the indirect one.

A final and useful quantity that can be compared to the experiment is the integrated spectral weight $\omega_P^2/8\pi$ which is related to $\langle K\rangle$ by the sum rule (14). Setting the lattice constant $a\approx 3$ Å the average V-V distance, we find that our results underestimate the experiment by about a factor of 2, which may possibly be due to the fact that our model does not consider degeneracy (inset of Fig. 6) (Ref. 47).

Before leaving this subsection we shall address an important question, not yet fully settled, that is the mechanism by which the insulating solution is destroyed. The destruction of the insulating state occurs at a point U_{c1} which may be different from the critical point $U_c\approx 3D$ that is associated to the breakdown of the metallic state as the interaction U is increased.[15,16] This issue is physically relevant because one can envision a situation where the magnetic order stabilizes the insulating solution over the metallic solution, but, due to a large degree of magnetic frustration, the insulating state is very close to the fully frustrated paramagnetic insulator. The destruction of the paramagnetic insulating state was discussed in Ref. 11 using IPT. Here we address this issue using exact diagonalization.

We first study the behavior of the gap in the one-particle excitation spectrum defined as the position of the lowest-energy pole (with non-negligible weight) in the Green function as a function of the number of sites included in the representation of the effective bath. Although the mean-field theory is strictly formulated in the thermodynamic limit, in practice, the representation of the bath by a finite number of orbitals introduces finite-size effects. The data shown in Fig. 6 were obtained from the extrapolation of results from finite-size cluster Hamiltonians H^{n_s} to the $n_s\to\infty$ system. The value for Δ is defined as twice the energy of the lowest frequency pole appearing in the Green function. In Fig. 8 we show the gap as a function of the interaction U in systems of $n_s=3$, 5, and 7 sites. Figure 9 contains similar results as a function of $1/n_s$ which show the good scaling of Δ, especially as the gap goes to zero as U is decreased. Thus this approach indicates a continuous closure of the gap at a critical value of the interaction $U_{c1}=2.15$.

We also investigate the behavior of the inverse moments of the spectral function defined as

$$m_{-n}=\int_0^\infty \frac{\rho(\epsilon)d\epsilon}{\epsilon^n}. \tag{18}$$

The behavior of these quantities give a more detailed picture of the transition. The local picture of the paramagnetic insulator is that of a spin embedded in an insulator. Hybridization with the bands of this insulator transfers spectral weight to high frequencies, but the spin remains well defined at low energies (even though with a reduced spectral weight) as long as there is a finite gap in the insulator. As U_{c1} is approached, and the gap decreases, we face the question whether the spin remains well defined even at the transition point. This depends on the behavior of the density of states

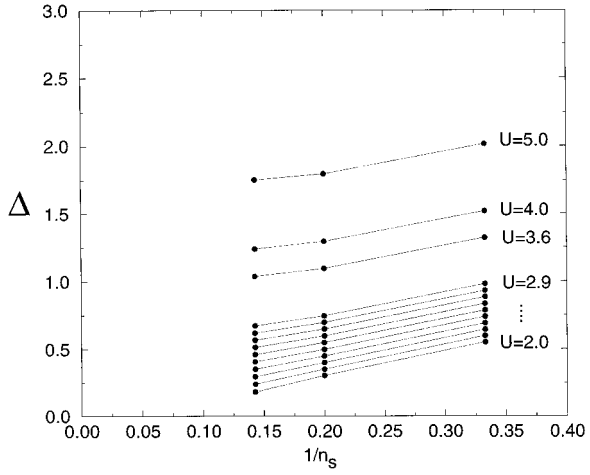

FIG. 9. The gap Δ vs the inverse of the number of sites $1/n_s$ in the paramagnetic insulator for various values of U. Δ is twice the energy of the lowest pole from the ED Green function.

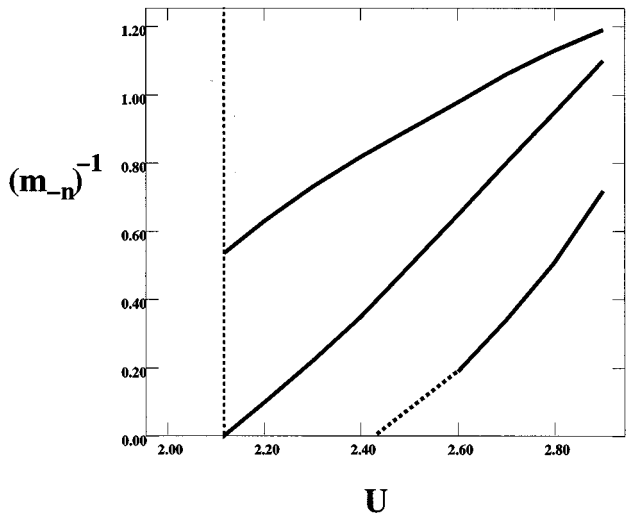

FIG. 10. Inverse of the first three inverse moments $(m_{-n})^{-1}$ of the density of states as a function of U. The three curves correspond from top to bottom to the inverse of the first, second, and third inverse moments respectively. The results are the $n_s \to \infty$ extrapolation from clusters of three, five, and seven sites, assuming $1/n_s$ scaling behavior. The dotted continuation of the last curve indicates results where the scaling is not reliable due to the strong divergent behavior of that inverse moment. The vertical dotted line indicates the value obtained for U_{c1} from the inverse moment analysis.

of the bath ρ_{bath} at low frequencies [we recall that ρ_{bath} is essentially ρ in a Bethe lattice; cf. Eq. (5)]. Whittoff and Fradkin[38] showed that if the density of states of the bath vanishes as a power law $\rho_{\text{bath}} \propto \epsilon^{\beta}$, the spin remains well defined if $\beta > 1$, while the spin is Kondo quenched if $\beta < 1$ and the spin degree of freedom is absorbed by the conduction electrons. The case $\beta = 1$ is marginal.

In a previous publication[16] we showed that within IPT the second inverse moment remains finite at the transition, while it diverges in the Hubbard III solution. Notice that m_{-2} can remain finite up to the transition even when the gap closes, but a divergent second inverse moment *implies* the continuous closure of the gap. In Fig. 10 we plot the *inverse* of m_{-2} together with that of the first and third inverse moments. The results correspond to the extrapolation to the infinite-size effective bath, performed similarly as was done previously for the gap. The inverse of the second inverse moment shows good scaling behavior with the system size, and is found to go to zero for $U \approx 2.12$. At this value of the interaction the moment diverges, which signals the breakdown of the insulating state, with the gap closing continuously. As expected, the first inverse moment remains finite at the transition (it also shows good scaling behavior), and, on the other hand, the inverse of the third inverse moment becomes negative even before the transition. This is due to the fast divergence of the third moment, which renders the finite-size scaling inaccurate. It is important to stress that this way of looking at the transition is very different from the previous one; nevertheless, the estimates for U_{c1} that are obtained after the infinite-size bath extrapolation are consistently predicted to within less than 2%. The results are substantially different from the ones obtained from IPT.

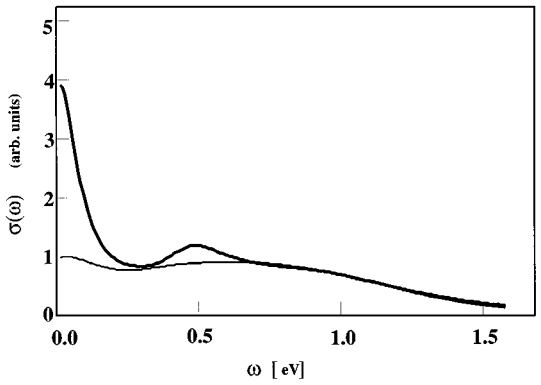

FIG. 11. The model $\sigma(\omega)$ for the metallic solution at $U = 2.1D$ and $T = 0.05D$ (upper) and $0.083D$ (lower). A small $\Gamma = 0.30$ and $0.5D$ was included to mimic a finite amount of disorder.

3. Metallic state

We now discuss the data of Thomas *et al.* in the metallic phase. In Fig. 4 at the beginning of this section, we reproduced experimental data for pure samples that become insulating below $T_c \approx 150$ K.[21] The spectra were obtained in the metallic phase at $T = 170$ and 300 K, and are made up of broad absorption at higher frequencies and some phonon lines in the far infrared. They appear to be rather featureless, however, upon considering their difference (in which the phonons are approximately eliminated) distinct features are observed. As T is lowered, there is an enhancement of the spectrum at intermediate frequencies of order 0.5 eV; and more notably, a sharp low-frequency feature emerges that extends from 0 to 0.15 eV. Moreover, these enhancements result in an anomalous *change* of the total spectral weight $\omega_P^2/8\pi$ with T. We argue below, that these observations can be accounted by the Hubbard model treated in mean-field theory.

In Fig. 11 we show the calculated optical spectra obtained from IPT for two different values of T. The interaction is set to $U = 2.1D$ that places the system in the correlated metallic state. It is clear that at least the qualitative aspect of the physics is already captured, and setting $D \approx 0.4$ eV we find these results consistent with the experimental data for V_2O_3 (Fig. 4). As the temperature is lowered, we observe the enhancement of the incoherent structures at intermediate frequencies of the order $U/2$ to U, and the rapid emergence of a feature at the lower end of the spectrum. These two emerging features can be interpreted from the qualitative picture that was discussed in Sec. III which is relevant for low T. From the model calculations with the parameters of Table I, we find the enhancement of the spectral weight taking place at a scale $T_{\text{coh}} \approx 0.05D \approx 240$ K which correlates well with the experimental data. T_{coh} has the physical meaning of the temperature below which the Fermi liquid description applies,[16] as the quasiparticle resonance emerged in the density of states.

In Fig. 12 we present the results for $\langle K \rangle$ as a function of the temperature. An interesting prediction of the model is the anomalous increase of the integrated spectral weight $\omega_P^2/8\pi$ as T is decreased. This feature is actually observed in experimental data, that show a notable difference between the in-

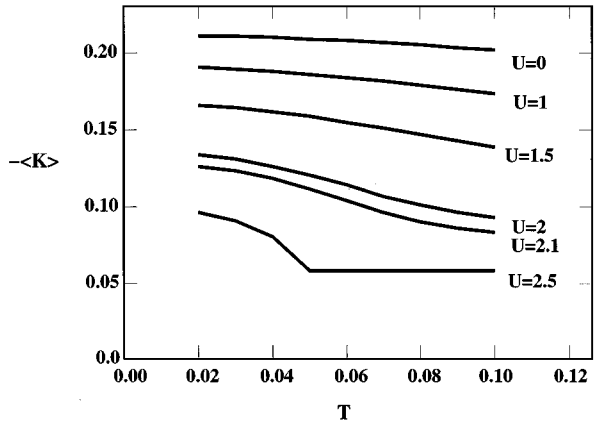

FIG. 12. Expectation value of minus the kinetic energy $\langle K\rangle$ as a function of the temperature for various U (IPT). This quantity is directly proportional to the optical conductivity sum rule. It predicts a notable *increase* in the optical spectral weight as the temperature is *decreased* in the correlated metallic regime.

tegrated spectral weight that persists up to the maximum frequencies measured ($\omega \approx 6$ eV). This effect is due to the rather strong T dependence of the kinetic energy $\langle K\rangle \propto \omega_P^2/8\pi$ in the region near the crossover associated with the first-order metal-insulator transition line that occurs in the phase diagram of the model.[21] This results from the competition between two small energy scales, namely, the temperature and the renormalized Fermi energy ϵ_F^*

Figure 13 contains the comparison between the results for the same quantity $\langle K\rangle$ at $U=2$ as obtained from the IPT and finite-temperature ED methods. This demonstrates that the temperature dependence is indeed a true feature of the model which is successfully captured by the approximate IPT solution.

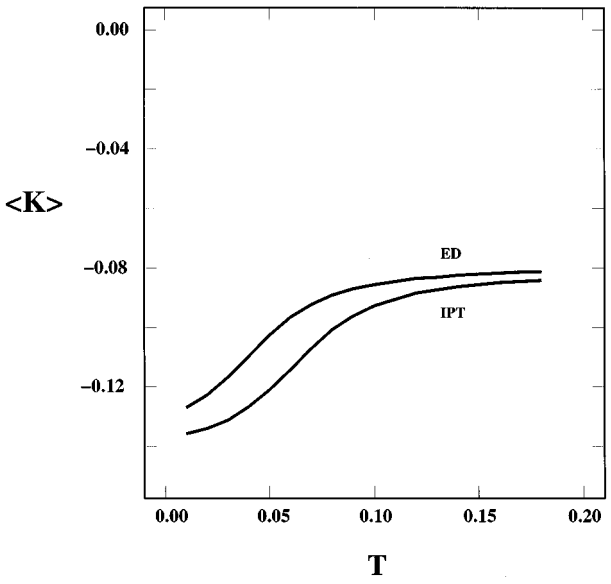

FIG. 13. Comparison of the expectation value of the kinetic energy $\langle K\rangle$ as a function of the temperature for $U=2$ as obtained from IPT and ED methods.

Although the qualitative aspect seems to be very accurately described by the model, we find $\omega_P^2/8\pi \approx 500$ eV/Ω cm which is lower than the experimental result. This could be due to the contribution from tails of bands at higher energies that are not included in our model, or it may indicate that the bands near the Fermi level are degenerate.

We now finally want to consider an important prediction of the model for the slope of the linear term in the specific heat γ in the metallic phase. Experiments show that the slope γ is in general unusually large. For 0.08, Ti substitution $\gamma \approx 40$ mJ/mol K^2, while for a pressure of 25 Kbar in the pure compound $\gamma \approx 30$ mJ/mol K^2 and with a V deficiency in a range of $y=0.013$ to 0.033 the value is $\gamma \approx 47$ mJ/mol K^2.[39] In our model, γ is simply related to the weight in the Drude peak in the optical conductivity and to the quasiparticle residue Z, $\gamma=(1/ZD)3$mJ eV/mol K^2. The values of $U=2.1D$ and $D\approx 0.4$ eV extracted from the optical data correspond to a quasiparticle residue $Z\approx 0.3$, and result in $\gamma \approx 25$ mJ/mol K^2 which is close to the experimental findings. Thus it turns out that the mean-field theory of the Mott transition explains, in a natural and qualitative manner, the experimentally observed optical conductivity spectrum, the anomalously large values of the slope of the specific heat γ, and the dc conductivity in the metallic phase, as a consequence of the appearance of a single small energy scale, the renormalized Fermi energy ϵ_F^*

4. Magnetically ordered solutions

Before leaving the Hubbard model and the V_2O_3 compound, we shall consider the important question of model solutions with magnetic long-range order (MLRO). In infinite dimensions the optical conductivity is a weighted convolution of two one-particle spectral functions. The one-particle spectral function is, therefore, the basic building block which gives rise to the various features of the optical conductivity. In this subsection we consider the nature of the spectral functions with MLRO. The understanding of the qualitative differences and similarities between solutions with and without MLRO is relevant in regard to systems, like V_2O_3, that present both antiferromagnetic (AFI) and paramagnetic (PI) insulating phases.

In Fig. 14 we show, respectively, the single-particle spectra of the PI and AFI insulating solutions for different values of the interaction U. The results are obtained from the ED method at $T=0$ for clusters of seven sites. The finite number of poles in the spectra correspond to the finite size of the clusters that can be practically considered. A finite broadening of the poles was added for better visualization.

In the AFI case, we plot the averaged value of the sublattice Green functions $\overline{G_\sigma}$,[40]

$$\overline{G_\sigma}=\tfrac{1}{2}(G_{A\sigma}+G_{B\sigma})=\tfrac{1}{2}(G_{A\sigma}+G_{A-\sigma}), \tag{19}$$

which is the quantity to be compared to photoemission experiments.

It is interesting to realize from these results, which correspond to rather large values of the interaction U, that the spectra in both cases are roughly similar. They both present a lower and upper Hubbard band at energies $\approx \pm U/2$ with a bandwidth $\approx 2D$ and a corresponding gap $\Delta \approx U-2D$.

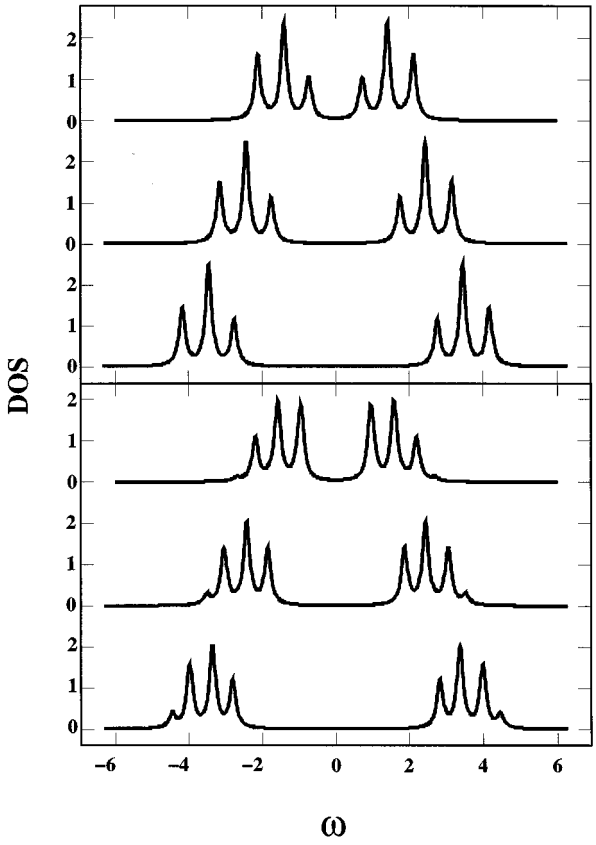

FIG. 14. Above: DOS of the paramagnetic insulator solution obtained from exact diagonalization of seven sites with $U=3$, 5, and 7 (top to bottom). A small broadening has been added to the poles. Below: idem for the antiferromagnetic insulator solution.

In particular, the PI solution merely presents a rigid shift of the incoherent Hubbard bands as the interaction U is varied, which is reminiscent of Hubbard's solution of the model.[13,41] On the other hand, in the AFI case, the shape of the density of states follows from the fact that the sublattice magnetization is basically saturated at these large values of the interaction.

At $U=7$, the largest value of the interactions considered, we observe that the shape of the spectra of G becomes very similar to the corresponding one in the disordered case. This can be understood from the fact that the magnetic exchange scale $J\sim D^2/U$ vanishes as U becomes large. As one decreases the strength of the interaction, we observe that the AFI spectra become increasingly different from the PI ones. In the former there is a transfer of spectral weight that occurs within the bands, from higher to lower frequencies. This is a consequence of the fact that, as the scale J becomes increasingly relevant, the spectra acquire a more coherent character. The ''piling up'' that occurs with the transfer of spectral weight as U is reduced is the precursor of the weak coupling inverse square root singularity in the low frequency part of the density of states. It is interesting to note that recent photoemission experiments in V_2O_3 report the presence of a small anomalous enhancement in the lower-frequency edge of the spectrum in the AFI phase. This feature may be interpreted from the previous results as evidence of the transfer of

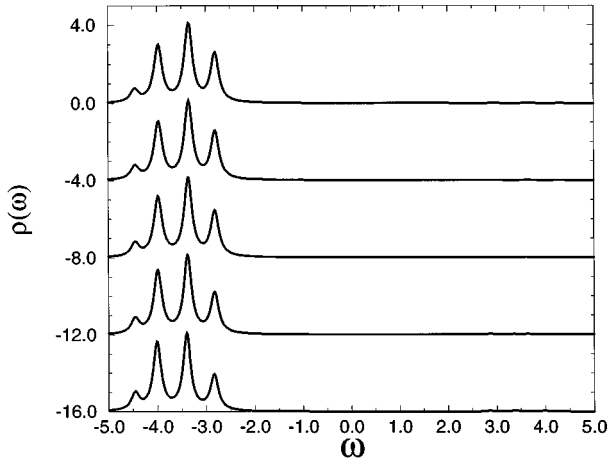

FIG. 15. ϵ-resolved single-particle spectra of the antiferromagnetic insulator solution obtained from exact diagonalization of 7 sites with $U=7$ with $\epsilon=0.0$, 0.25, 0.5, 0.75, and 1.0 (top to bottom). A small broadening $\eta=0.1$ was added to the poles, and the figures were vertically shifted for better visualization.

weight within the Hubbard bands, corresponding to a case of an intermediate degree of frustration.

A complementary perspective on the results that we just discussed is obtained by looking at the k-resolved spectra given by the imaginary part of the Green function $G(k,\omega)$, which reads

$$G(k,\omega)=\frac{1}{\omega-\epsilon_k-\Sigma(\omega)}. \tag{20}$$

In the large-d limit the energy ϵ_k that enters in the Green functions loses its explicit k dependence.[7] Nevertheless, one can still think of this quantity as analogous to the k-resolved spectra if one notes that the ϵ goes from $-D$ to D as it traverses the band (the dispersion is linear in the noninteracting case). In Figs. 15 and 16 we show the

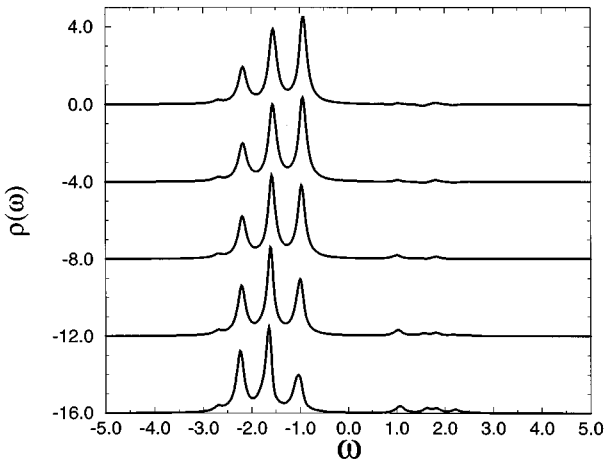

FIG. 16. ϵ-resolved single-particle spectra of the antiferromagnetic insulator solution obtained from exact diagonalization of seven sites with $U=3$ with $\epsilon=0.0$, 0.25, 0.5, 0.75, and 1.0 (top to bottom). A small broadening $\eta=0.1$ was added to the poles, and the figures were vertically shifted for better visualization.

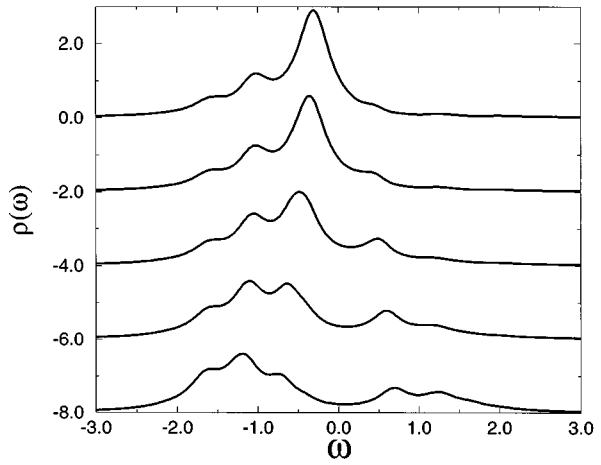

FIG. 17. ϵ-resolved single-particle spectra of the antiferromagnetic insulator solution obtained from exact diagonalization of seven sites with $U=1.5$ with $\epsilon=0.0$, 0.25, 0.5, 0.75, and 1.0 (top to bottom). A small broadening $\eta=0.2$ was added to the poles, and the figures were vertically shifted for better visualization.

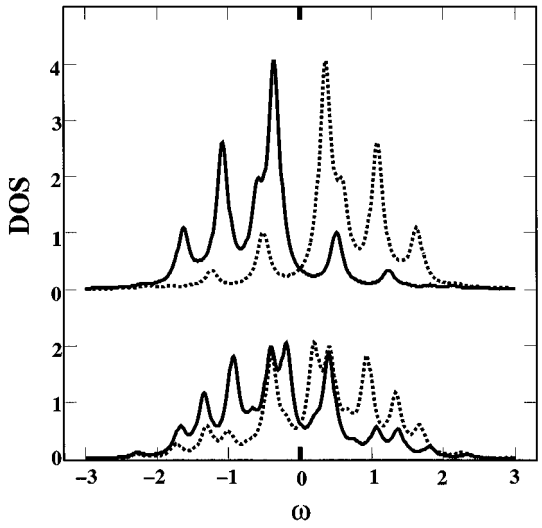

FIG. 18. DOS obtained from exact diagonalization of seven sites with $U=1.5$ for $(t_2/t_1)=0$ (top) and $(t_2/t_1)=\sqrt{1/3}$ (bottom). A small broadening $\eta=0.1$ was added to the poles.

ϵ-resolved spectra for the different values of the interaction considered before. From the inspection of the spectra we observe that in the low J case for $U=7$ the single-particle spectra remain basically unmodified as we scan the ϵ ''wave vectors,'' which indicates the very incoherent character of the single-particle excitations. On the other hand, as we lower U and the scale J becomes larger, we note the emergence of a peak in the $U=3$ case for small values of ϵ, that indicates its coherent character.

Upon further reduction of the strength of the interaction U, as we show in Fig. 17 for $U=1.5$, we find that the coherent features of the spectra begin to acquire *dispersion*. This is observed, not only in the ''particle'' ($\omega<0$) but also in the emerging ''hole'' part of the spectra, as the size of the staggered magnetization decreases. These results display a striking similarity to the physics found in recent finite dimensional finite lattice size QMC calculations by Preuss, Hanke, and van der Linden.[42]

We can summarize the previous results by saying that the ED solutions indicate that, as the lattice becomes unfrustrated (nested) and as U/t is reduced, the spectral function of the insulating state develops more dispersion, and the excitations at low energy become more coherent (i.e., the imaginary part of the self-energy is smaller). As we argued above, many experiments place V_2O_3 in the opposite regime of strong frustration; however, the observation of dispersive features in the insulating phase of $NiS_{1.5}Se_{0.5}$ (Ref. 43) may be explained by a lower degree of magnetic frustration in this compound.

It should now be clear that an important parameter of the theory is the degree of magnetic frustration. Thus a final topic that we shall briefly consider is the case of solutions with MLRO in a model with an intermediate degree of frustration. The degree of frustration can be controlled in our model by adding to the original Hamiltonian, with nearest-neighbor hopping t_1, a next-nearest-neighbor hopping amplitude t_2.[16] In order to maintain the half-bandwidth $D=2t$ fixed and the bare density of states ρ^0 invariant, one has to keep $t_1^2+t_2^2=t^2$. Note that for $t_2/t_1=0$ we recover the original Hamiltonian, and $t_2/t_1=1$ gives the paramagnetic solution. The extra hopping provides a magnetically frustrating interaction by lifting the rather artificial nesting property of the original model.

In a recent letter,[21] we showed that the inclusion of finite frustration in the original model Hamiltonian is essential in order to reproduce the main qualitative features and the precise topology of the phase diagram of V_2O_3. In particular we found a small region in the phase diagram which corresponds to an antiferromagnetic metallic state (AFM). In Fig. 18 we show the density of states for $t_2/t_1=0$ (AFI), and $t_2/t_1=\sqrt{1/3}$ (AFM) with the interaction $U=1.5$. The results obtained from seven sites show exact diagonalization. It is very interesting to note that the peak structure of the density of states seems to be divided into low-frequency features near $\omega=0$, and higher-frequency structures at energies of the order of the bandwidth (which is also comparable to U for the chosen parameters). This is even more clear in the antiferromagnetic metallic state with partial frustration. We note that our results are qualitatively similar to the recent results by Moreo *et al.*[44] obtained in exact diagonalization of the t-J model and also quantum Monte Carlo results for the Hubbard model on two-dimensional finite-size lattices with a choice of parameters comparable to the one used here.[44]

We conclude this subsection with an important technical remark: in order to apply the exact diagonalization method of Ref. 18 to the problem with intermediate frustration $0<t_2/t_1<1$, it is necessary to be able to average the continued fractions for the spin-up and spin-down Green functions into a single continued fraction. To perform this task we use the algorithm detailed in the Appendix.

B. Periodic Anderson model

In this section we shall consider the predictions of the periodic Anderson model within the present dynamical mean-field theory in the context of several questions which emerge from the experimental data on Kondo insulator systems $Ce_3Bi_4Pt_3$ (Ref. 2) and FeSi.[3] In particular we shall

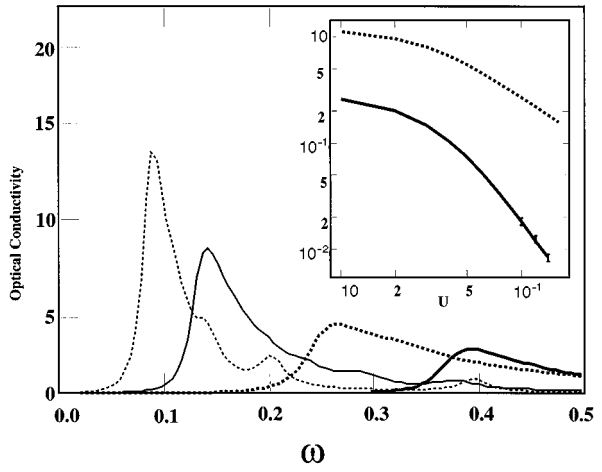

FIG. 19. The optical conductivity spectra of the periodic Anderson model for values of the interaction $U=0.5$, 1, 2, and 3 (right to left), keeping the hybridization $V=0.25$ fixed. The inset shows the gap from the optical spectra $\Delta_c \approx \Delta_{\rm dir}$ and the indirect gap $\Delta_{\rm ind}$ from the local density of states for $V=0.6$. The slopes of these curves indicate that $V^{*2}/D \propto \Delta_{\rm ind}$ and $V^* \propto \Delta_{\rm dir}$ in the strong-correlation region.

address the following issues: (i) the energy scales that are involved in the formation of the gaps; (ii) the temperature dependence of the integrated optical spectral weight as the gap forms; and (iii) the scattering rate.

1. Gap formation

Kondo insulators are a second class of systems where the correlations induce an anomalous temperature dependence. While the most qualitative physics of these systems is well understood, several features remain puzzling.[20] The charge gap Δ_c measured in optical conductivity is larger than the spin gap Δ_s measured in neutron scattering.[2] Also, the transport gap Δ_t obtained from the activation energy in dc transport measurements is smaller than Δ_c. On the other hand, from recent optical experiments on $Ce_3Bi_4Pt_3$ (Ref. 2) and FeSi,[3] we can distinguish some common features regarding the energy scales associated with the formation of the optical gap. The gap Δ_c begins to open at a characteristic temperature $T^* \sim \Delta_c/5$ and becomes fully developed at a much smaller temperature of the order of $T^*/5$. Also, the gap is temperature independent below T^*. In $Ce_3Bi_4Pt_3$, it is found that $\Delta_c \approx 450$ K, $\Delta_s \approx 250$ K, and $T^* \approx 100$ K, and the optical gap is completely depleted only below ≈ 25 K.[2] On the other hand, qualitatively similar results were reported for FeSi, with $\Delta_c \approx 1000$ K, and $T^* \approx 200$ K, and the gap becomes depleted between 20 and 100 K.[3]

The mean-field theory accounts for all these observations. The low-energy behavior of the one-particle Green functions of the model can be understood as that of a noninteracting system, where the interaction U reduces the hybridization from its bare value V to a renormalized value V^* which decreases as U increases. As a consequence, the gap in the optical conductivity decreases by the effect of correlations. However, the line shape remains approximately invariant, and is merely changed by a rescaling factor with respect to the response of the noninteracting model. This is demonstrated by the plot of the optical conductivity $\sigma(\omega)$ for different values of U shown in Fig. 19. The optical gap Δ_c is given by the *direct gap* $\Delta_{\rm dir}$ of the renormalized band structure. These results were obtained by IPT at $T=0$, and we checked in various cases that the results are in excellent agreement with the ED method.

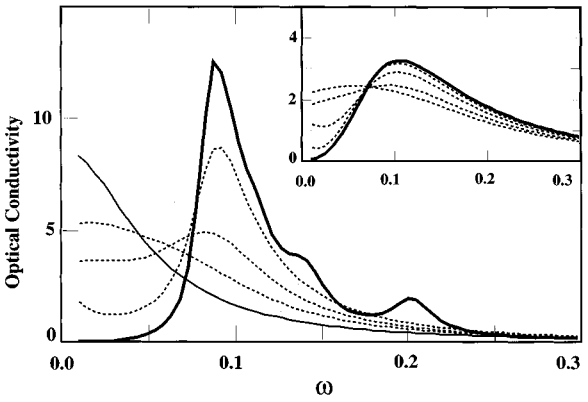

FIG. 20. The optical conductivity for the Anderson model at $T=0.001$ (bold), 0.005, 0.01, 0.02 (dotted), and 0.03 (thin). The interaction $U=3$ and $V=0.25$. Inset: The same quantity at $T=0.001$ (bold), 0.005, 0.01, 0.02 (dotted), and 0.03 (thin) with Lorentzian random site disorder of width $\Gamma=0.05$.

We now consider the behavior of $\sigma(\omega)$ with temperature. Figure 20 shows the optical conductivity for different temperatures with the parameters $U=3$ and $V=0.25$ fixed. The gap is essentially temperature independent. It begins to form at $T^* \approx 0.02 \sim \Delta_c/5$, and is fully depleted only at temperatures of the order of $T^*/5$. We thus observe that the mean-field theory is able to capture the qualitative aspect of the experimental results that we summarized above. This basically consists in the individualization of three different energy scales: a large one which corresponds to the gap of the

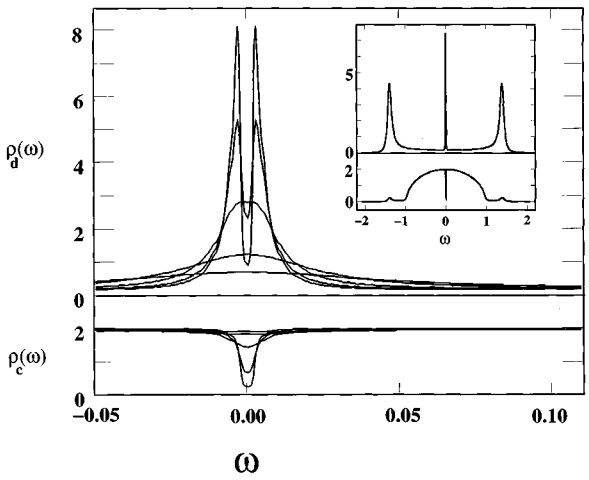

FIG. 21. Low-frequency part of the density of states for the d and c electrons (top and bottom) obtained from IPT at $T=0.001$, 0.005, 0.01, 0.02, and 0.03 for $U=3$ and $V=0.25$ (top to bottom for d electrons and bottom to top for c electrons). Inset: The density of states in the full frequency range at $T=0.001$.

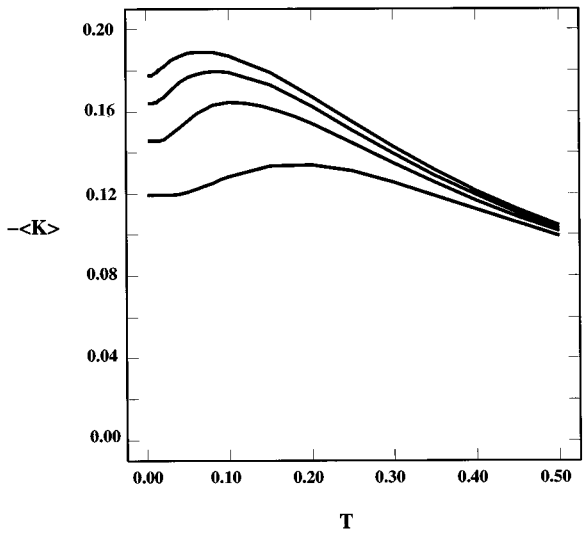

FIG. 22. Expectation value minus the kinetic energy $\langle K\rangle$ as a function of the temperature for $U=0,\ 2,\ 3,\ 4$, and $V=0.4$ (bottom to top) as obtained from IPT. This quantity is directly related to the optical conductivity sum rule. It predicts a notable *decrease* in the total optical spectral weight as the temperature is *decreased* in the range below the maxima.

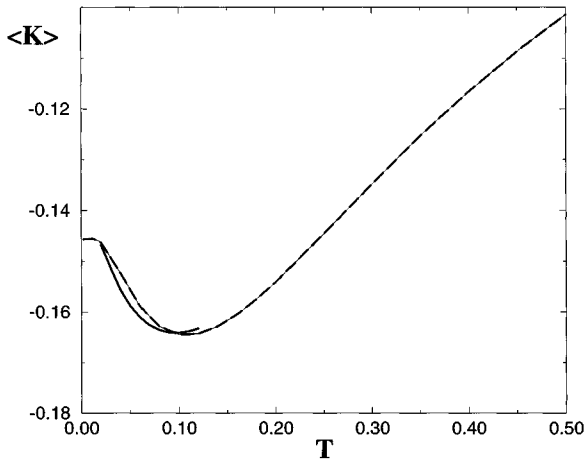

FIG. 23. Comparison of the expectation value of the kinetic energy $\langle K\rangle$ in the PAM as a function of the temperature for $U=2$ and $V=0.4$ as obtained from IPT and ED methods (dashed line and full line).

optical spectra $\Delta_c\sim\Delta_{\rm dir}$, an intermediate scale $T^*\sim\Delta_c/5$, where this gap starts to form and quasiparticle features start to appear in the DOS; and a third and smaller scale $\Delta_{\rm ind}\sim T^*/5$, which corresponds to the temperature where the optical gap is completely depleted. As demonstrated in Fig. 21, where we plot the results for the density of states, the small scale $\Delta_{\rm ind}$ also indicates the temperature below which the gap in the density of states opens, and, thus, can be associated with the gap measured in dc-transport experiments Δ_t. This last feature, and the fact that $\Delta_{\rm ind}\sim\Delta_t\ll\Delta_{\rm dir}\sim\Delta_c$, accounts for one of the experimental observations mentioned above.

In order to make a meaningful comparison with the experimental data, we have added the effects of disorder by putting a Lorentzian distributed random site energy on the conduction-electron band with width $\Gamma=0.05$. The results are displayed in the inset of Fig. 20, and they show that the introduction of disorder places the overall shape of the spectra in closer agreement with the experimental results[2,3] (for a discussion of the scattering involved, see Sec. IV B 2). Also, we observe that increasing the disorder *reduces* the temperature T^*.

In the following, we briefly address the question of the integrated total spectral weight. It has been noted that experimental results for both $Ce_3Bi_4Pt_3$ and FeSi, seem to violate the sum rule for the spectral weight.[2,3] However, this point has been recently questioned, at least for the FeSi compound.[45] In order to contribute to the proper interpretation of the experimental data, it is important to compute the kinetic energy of our model at finite temperature, which is directly related to the sum rule of Eq. (14). The results from IPT are presented in Fig. 22, which shows the notable dependence of the kinetic energy with temperature and interaction strength [we plot the negative of $\langle K\rangle$ which is the quantity that enters Eq. (14)]. In Fig. 23, we plot similar results obtained with the ED algorithm, which demonstrates that the behavior captured by the IPT calculation is indeed a true feature of the model.

As we previously discussed for the the Hubbard model case, the strong correlation effects that renders $\langle K\rangle$ a function of the temperature implies that *if the PAM is the relevant model for the systems at low energies*, then the results predict the behavior of the integrated optical weight within the low-frequency range. Actually, experimental data, which are inferred from the Kramers-Kronig transformation of reflectivity measurements, can only be reliably obtained within a limited low-frequency range of the order of a few eV. The behavior of $\langle K(T)\rangle$ in Fig. 23 is *nonmonotonic*. As we increase the temperature from zero, we observe initially that the kinetic energy decreases. This is a consequence of electron delocalization, since the system becomes a metal as the small gap in the density of states is filled. The kinetic energy then goes through a minimum and starts to increase as the temperature is further increased. This is due simply to the thermal excitation of electrons within the single conduction band. Correlations now play an irrelevant role, as the temperature is higher than the coherence temperature T^*. When we study the behavior for different values of the interaction U in Fig. 22, we observe that the position of the minima (maxima in this figure as $-\langle K(T)\rangle$ is plotted), becomes smaller as U is increased. This can be understood simply as a consequence of the renormalization of the hybridization amplitude $V\rightarrow V^*$.

In regard to the experimental situation in the Kondo insulators, which indicate the apparent violation of the optical sum rule, our results give a plausible qualitative explanation for the observed behavior. In fact, for experimental data obtained at temperatures smaller than the size of the gap Δ_c and *restricted to a finite low-frequency range* (which indeed corresponds to the actual situation), the model predicts the apparent ''disappearance'' of spectral weight as the temperature is decreased.

We should also point out that although this simple model accounts, rather successfully, for the various energy scales, it fails to provide an accurate reproduction of the detailed ex-

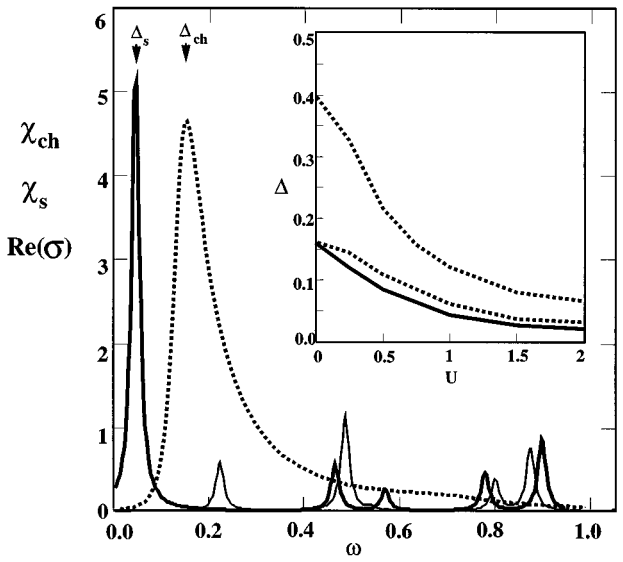

FIG. 24. The local spin-spin (bold) and charge-charge (thin) susceptibility from seven ED sites. The optical conductivity from IPT (dotted). The parameters are $U=1$ and $V=0.2$. The y axis is in arbitrary units. Inset: The direct gap from IPT (upper dotted line), the indirect gap (lower dotted line), and the spin gap (solid line) from eight ED sites. The hybridization is $V=0.2$.

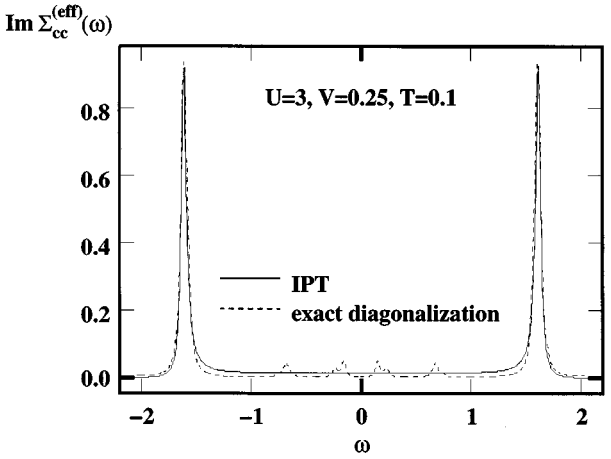

FIG. 25. $\mathrm{Im}\Sigma_{cc}^{(\mathrm{eff})}(\omega)$ for $U=3$, $V=0.25$, and $T=0.1$ ($D=1$). The results are from ED (dashed line) and IPT (full line) methods.

perimental line shape. A complete explanation of the experimental results may need the consideration of additional sources of scattering, as will be discussed in Sec. IV B 2.

To finish our discussion about gap formation in the periodic Anderson model, we shall present the results for the size of the various gaps that are obtained from the correlation functions. The first study of the periodic Anderson model in large dimensions was carried out by Jarrell, Akhlaghipour, and Pruschke using the quantum Monte Carlo method.[22] Our spectral functions and density of states are in general agreement with the early work in the region where the QMC and exact diagonalization methods can be compared. A noticeable qualitative difference is that we find the spin gap to be slightly but strictly smaller than the indirect gap when $U\neq 0$.

In Fig. 24 we show the local spin- and charge-correlation functions along with the optical conductivity, which shows qualitative agreement with the experimental data of Ref. 2. We also compare in the inset the direct optical gap Δ_{dir}, the indirect gap Δ_{ind} relevant for transport properties, and the spin gap Δ_s obtained from the spin-spin-correlation function. We find that Δ_{dir} is consistently larger than Δ_s, and that Δ_s is somewhat smaller than Δ_{ind}. As expected when $U=0$, $\Delta_s=\Delta_{\mathrm{ind}}$, but, as U increases, $\Delta_s/\Delta_{\mathrm{ind}}$ becomes smaller than unity and approaches the value 1/2 at $U\approx 2$.

2. Scattering rate

In the previous subsection we stressed the qualitative success of the mean-field theory of the periodic Anderson model in connection with the gap formation in Kondo insulators like FeSi and $Ce_3Bi_4Pt_3$. In this section, however, we will show that this approach *cannot* account for the large scattering rate measured in these materials, if one does not include the effects of disorder in the model. This is very surprising, and is an indication of the limitations of the one-band periodic Anderson model for modeling these systems.

The optical conductivity of Kondo insulators is — except for the gap which forms at low temperatures — almost constant over a large frequency range extending to several times the width of the gap. The corresponding value of $\sigma(\omega)$ is quite similar for all of the materials [typically 3000–4000 $(\Omega\,\mathrm{cm})^{-1}$], and depends only weakly on temperature. The related scattering rate can be estimated (at $T>T^*$) by simple Drude model arguments: at zero frequency, we have $\sigma=ne^2\tau/m$. Here $n=a^{-3}$, where a denotes the lattice constant. m can be obtained from the kinetic energy $p^2/2m\approx D$, where $p\approx 2\pi\hbar/a$. Assuming $a\approx 10^{-10}m$, the equations yield $\hbar/\tau\sim\sigma_0^{-1}10^3(\Omega\,\mathrm{cm})^{-1}D$. Thus the measured values for σ_0 imply a scattering rate which is of the order of the bandwidth ($1/\tau\sim D$, assuming $\hbar=1$). This should be compared with the scattering rate found in normal metals like copper, which is three orders of magnitude smaller ($1/\tau\sim 10^{-3}D$).

Since all experiments on Kondo insulators (and also on many Kondo metals) observe (above the gap) the same order of magnitude for $\sigma(\omega)$, one should expect that there is a common mechanism involved. It is reasonable to assume that the scattering of conduction electrons by the localized electrons in the periodic Anderson model provides an explanation. To address this question, we calculated the effective scattering rate. This quantity is determined by the effective c-electron self-energy $\Sigma_{\mathrm{cc}}^{(\mathrm{eff})}$

$$\Sigma_{\mathrm{cc}}^{(\mathrm{eff})}(\omega)=\frac{V^2}{\omega+\mu-\Sigma_{dd}(\omega)}, \tag{21}$$

where Σ_{dd} is the self-energy of the localized d electrons, which enters the formula for the optical conductivity (13) via $A_{\epsilon_k}(\omega)=-2\,\mathrm{Im}1/[\omega+\mu-\epsilon_k-\Sigma_{cc}^{(\mathrm{eff})}(\omega)]$. The imaginary part of $\Sigma_{cc}^{(\mathrm{eff})}(\omega)$ measures the scattering involved. In Fig. 25 we plotted this quantity for the particle-hole symmetric case, $V=0.25D$, $U=3D$, and $T=0.1D$. Since in this section we are not interested in the gap formation, the temperature was chosen to be well above the point where the gap starts to open ($T^*\approx 0.025D$). For comparison, the calculation was

done with both the ED and IPT. It is clear from the plot that the scattering rate is much smaller than the bandwidth D, and gives rise to an optical conductivity which is smaller than the experimentally observed value by two orders of magnitude. This result remains valid away from particle-hole symmetry, and for different choices of V and U. If one ignores the self-consistency condition, one would expect, based on the theory of the Kondo impurity model, that, as the temperature is lowered the scattering rate should grow toward the unitary limit D. This growth, which is expected at low frequencies and low temperatures, is preempted in the lattice by the formation of the hybridization gap.

For $V/U \ll 1$ and half-filling, the periodic Anderson model can be transformed into a Kondo lattice model by a Schrieffer-Wolff transformation

$$H_{\mathrm{KL}}=\frac{D}{2}\sum_{<ij>,\sigma} c^{\dagger}_{i\sigma}c_{j\sigma}+J\sum_{i,\sigma\sigma'}\vec{S}_i c^{\dagger}_{i\sigma}\vec{\tau}_{\sigma,\sigma'}c_{i\sigma'}, \qquad (22)$$

where $J=8V^2/U$. Here $\vec{S}_i$ describes a spin at site i. For a cross-check, we also examined this Hamiltonian using the exact diagonalization method. For $J=\frac{1}{6}D$, which corresponds to $V=0.25D$ and $U=3\,D$, we find at $T=0.1D$ a scattering rate $1/\tau \sim -\,\mathrm{Im}\Sigma_{cc}(\omega=0)\approx 7\times 10^{-3}D$. This is again much less than required to explain the experimental data.

We believe that the failure observed here within the present approach is a general shortcoming of the periodic Anderson model. A more realistic description has to take several crystal-field-split bands and this could increase the finite frequency optical absorption.

V. CONCLUSIONS

In this paper we have illustrated how the LISA, that becomes exact in the limit of large dimensions, can be used to study the physics of systems where the local interactions are strong and play a major role. In particular we have demonstrated that the Hubbard and periodic Anderson models, treated within this dynamical mean-field theory, can account for the main features of the temperature-dependent transfer of spectral weight in the optical conductivity spectra. In the case of V_2O_3, we found that the theory is able to account semiquantitatively for the conductivity results in both the metallic and insulating states. Also, in the metal, it explains the unusually large values observed in the slope of the specific heat γ. In the insulating phase, the theory seems to provide further insight into the role of the magnetic frustration. In this regard, we studied in detail the predictions of the model for the photoemission spectra when long-range order is present, and noted that the mean-field theory indeed captures many aspects of the behavior that was already encountered in numerical studies of the model in low dimensions.

For Kondo insulators, we have seen many of the qualitative features of the observed behavior of optical spectra, with the temperature captured by our model treated in mean-field theory. In particular, we identified the different energy scales associated with the formation of the optical gap, and how they are related to changes in the single-particle spectra. However, we saw that the periodic Anderson model is not able to explain the high scattering rate measured in Kondo insulators.

We also presented results for the temperature dependence of the optical sum rule in strongly correlated models. In the Hubbard model case, the results capture the qualitative decrease of the total spectral weight with increasing temperature that is experimentally observed in the V_2O_3 system. On the other hand, our results for the PAM may be relevant for the resolution of the ''missing'' spectral weight controversy in optical experiments on the insulators $Ce_3Bi_4Pt_3$ and FeSi.[2,3,45] From a broader perspective it has turned out to be very illuminating to realize how the emergence of a small ''Kondo'' energy scale in both, Hubbard and periodic Anderson models, results in the unusual temperature dependence of the projected optical sum rule [cf. Eq. (14)]. The appearance of a Kondo scale in these models is due to the fact that within the LISA, both lattice problems are mapped onto an Anderson single impurity. However, since they are subject to different self-consistency conditions, the temperature behavior of the solutions is very different. We have shown that in the Hubbard model case the optical weight increases when the temperature is reduced, and the system becomes more metallic, while in the periodic Anderson model it decreases, as a consequence of the system opening a gap and becoming insulating.

We finally stress that our mean-field approach can be easily adapted to incorporate more realistic band-structure densities of states and more complicated unit cells. These extensions would possibly allow for a more precise quantitative description of these interesting systems.

ACKNOWLEDGMENTS

We acknowledge valuable discussions with V. Dobrosavljevic, A. Georges, L. Laloux, E. Miranda, G. Moeller, Q. Si, and G. Thomas. This work was supported by the NSF under Grant Nos. DMR 92-24000 and 95-29138. Unité propre du CNRS, associée à l'Ecole Normale Supérieure et à l'Université de Paris Sud.

APPENDIX: ADDITION OF TWO CONTINUED FRACTIONS

In this appendix we present an algorithm that allows to sum two continued fractions into a single one. This is necessary for the implementation of the ED method in models with magnetic frustration or disorder, where various Green functions have to be averaged and the result has to be expressed as a continued fraction. The details of the ED method can be found in Ref. 18.

In the ED method an effective cluster Hamiltonian H^{n_s} of n_s sites is diagonalized. At $T=0$ only the ground state $|gs\rangle$ and the ground-state energy E_0 need to be obtained, and this can be efficiently done by the modified Lanczos method.[46] The local Green function $G(\omega)$ is then obtained as a continued fraction. Actually one needs to compute two continued fractions $G^{<}(\omega)$ and $G^{>}(\omega)$, for $\omega<0$ and for $\omega>0$, respectively.

$$G(\omega)=G^{>}(\omega)+G^{<}(\omega)$$
$$=\left\langle gs\left|c\frac{1}{\omega-(H^{n_s}-E_0)+i\delta}c^{\dagger}\right|gs\right\rangle$$
$$+\left\langle gs\left|c^{\dagger}\frac{1}{\omega+(H^{n_s}-E_0)+i\delta}c\right|gs\right\rangle, \quad \text{(A1)}$$

with

$$G^{>}(\omega)=\cfrac{\langle gs|cc^{\dagger}|gs\rangle}{\omega-a_0^{>}-\cfrac{b_1^{>2}}{\omega-a_1^{>}-\cfrac{b_2^{>2}}{\omega-a_2^{>}-\cdots}}}, \quad \text{(A2)}$$

$$G^{<}(\omega)=\cfrac{\langle gs|c^{\dagger}c|gs\rangle}{\omega-a_0^{<}-\cfrac{b_1^{<2}}{\omega-a_1^{<}-\cfrac{b_2^{<2}}{\omega-a_2^{<}-\cdots}}},$$

where c and $c^{\dagger}$ are the operators associated with the local site of H^{n_s}. The parameters $a_i^{>/<}$ and $b_i^{>/<}$ define the continued fractions, and are obtained from the following iterative procedure:

$$a_i^{\alpha}=\langle f_i^{\alpha}|H^{n_s}|f_i^{\alpha}\rangle, \quad b_i^{\alpha 2}=\frac{\langle f_i^{\alpha}|f_i^{\alpha}\rangle}{\langle f_{i-1}^{\alpha}|f_{i-1}^{\alpha}\rangle}, \quad \text{(A3)}$$

where $\alpha=>,<$ and $|f_0^{>}\rangle=c^{\dagger}|gs\rangle$, $|f_0^{<}\rangle=c|gs\rangle$, and

$$|f_{i+1}^{\alpha}\rangle=H^{n_s}|f_i^{\alpha}\rangle-a_i^{\alpha}|f_i^{\alpha}\rangle-b_i^{\alpha 2}|f_{i-1}^{\alpha}\rangle, \quad \text{(A4)}$$

and in the beginning we set $b_0^{\alpha}=0$.

Thus we observe that the basis defined by the vectors $|f_i^{\alpha}\rangle$ gives a *tridiagonal* representation of H^{n_s} which contains the a_i's along the main diagonal and the $\sqrt{b_i}$'s along the diagonals next to the main one. In the following we drop the index α to simplify the notation. We will explicitly restore it in the final result.

Let us now address the problem of our current interest. We assume that we have computed two Green functions $G_{\mu}(\omega)$, where the index μ may label, for instance, a spin. Our task is to obtain a continued fraction representation of the *average* Green function $\overline{G}(\omega)=\frac{1}{2}[G_{\uparrow}(\omega)+G_{\downarrow}(\omega)]$. The more general case of a weighted average can be trivially generalized from the present case which we consider for simplicity.

We first note that, from the Lanczos procedure, H^{n_s} has (different) *tridiagonal* representations in the two sub-bases defined by $|f_{i\mu}\rangle$ (we have dropped the $>,<$ label to simplify the notation). The representation is basically a matrix that contains parameters $a's$ along the main diagonal and $b's$ along the two subdiagonals.

The algorithm is as follows: one first diagonalizes the two tridiagonal representations of H^{n_s} by computing all the eigenvalues and eigenvectors. This is not numerically costly since the matrices are in tridiagonal form and it may be done by standard methods.

An important result that can be easily demonstrated is that the eigenvalues ϵ_{μ}^{ν} of the tridiagonal matrices are the poles of their corresponding Green functions $G_{\mu}(\omega)$. Furthermore, one can also show that

$$G_{\mu}(\omega)=\sum_{\nu=1}^{M}\frac{(v_{\mu}^{\nu})^2}{\omega-\epsilon_{\mu}^{\nu}}, \quad \text{(A5)}$$

where v_{μ}^{ν} are the first component of the M eigenvectors of the tridiagonal matrices.

Thus, from the definition of the Green function, one immediately recognizes that the vector $\{v_{\mu}^1,v_{\mu}^2,\ldots,v_{\mu}^M\}$ is nothing but $c_{\mu}^{\dagger}|gs\rangle$ expressed in a basis where H^{n_s} is diagonal (which is a sub-basis of the given sector's Hilbert space).

The final step consists of writing the Hamiltonian in the bases direct product of the two sub-bases, which, of course, will also be a diagonal representation of H^{n_s}; and then bring it to its tridiagonal representation through steps (A3) and (A4) starting from the vector defined by (restoring the $>,<$ label)

$$|f_0^{>}\rangle=(c_{\uparrow}^{\dagger}+c_{\downarrow}^{\dagger})|gs\rangle$$
$$=\vec{v}_{\uparrow}\oplus\vec{v}_{\downarrow}$$
$$=\{v_{\uparrow}^1,v_{\uparrow}^2,\ldots,v_{\uparrow}^M,v_{\downarrow}^{M+1},v_{\downarrow}^{M+2},\ldots,v_{\downarrow}^{2M}\}. \quad \text{(A6)}$$

Thus the newly determined $a_i^{>}$'s and $b_i^{>}$'s that result from this last step are the parameters of the continued fraction representation of $G^{>}(\omega)$ (the parameters for $G^{<}$ are obtained in a completely analogous manner).

*Present address: ILL, Ave. des Martyrs, B.P. 156, 38042 Grenoble Cedex 9, France.

[1] G. A. Thomas *et al.*, Low Temp. Phys. **95**, 33 (1994).
[2] B. Bucher, Z. Schlesinger, P. C. Canfield, and Z. Fisk, Phys. Rev. Lett. **72**, 522 (1994); B. Bucher *et al.*, Physica B **199&200**, 489 (1994).
[3] Z. Schlesinger, Z. Fisk, H. T. Zhang, M. B. Maple, J. F. DiTusa, and G. Aeppli, Phys. Rev. Lett. **71**, 1748 (1993).
[4] M. A. van Veenendaal and G. A. Sawatzky, Phys. Rev. Lett. **70**, 2459 (1993); Phys. Rev. B **49**, 3473 (1994).
[5] A. J. Millis, in *Physical Phenomena at High Magnetic Fields*, edited by E. Manousakis *et al.* (Addison-Wesley, Reading, MA, 1991), and references therein.
[6] For a recent review, see A. Georges, G. Kotliar, W. Krauth, and M. J. Rozenberg, Rev. Mod. Phys. **68**, 13 (1996).
[7] W. Metzner and D. Vollhardt, Phys. Rev. Lett. **62**, 324 (1989).
[8] A. Georges and G. Kotliar, Phys. Rev. B **45**, 6479 (1992).
[9] A. Georges, G. Kotliar, and Q. Si, Int. J. Mod. Phys. B **6**, 705 (1992).
[10] M. Jarrell, Phys. Rev. Lett. **69**, 168 (1992).
[11] M. J. Rozenberg, X. Y. Zhang, and G. Kotliar, Phys. Rev. Lett. **69**, 1236 (1992).
[12] A. Georges and W. Krauth, Phys. Rev. Lett. **69**, 1240 (1992).
[13] X. Y. Zhang, M. J. Rozenberg, and G. Kotliar, Phys. Rev. Lett. **70**, 1666 (1993).
[14] Th. Pruschke, D. L. Cox, and M. Jarrell, Phys. Rev. B **47**, 3553 (1993).
[15] A. Georges and W. Krauth, Phys. Rev. B **48**, 7167 (1993).
[16] M. J. Rozenberg, G. Kotliar, and X. Y. Zhang, Phys. Rev. B **49**, 10 181 (1994).

[17] M. Caffarel and W. Krauth, Phys. Rev. Lett. **72**, 1545 (1994).
[18] Q. Si, M. Rozenberg, G. Kotliar, and A. Ruckenstein, Phys. Rev. Lett. **72**, 2761 (1994); M. J. Rozenberg, G. Moeller, and G. Kotliar, Mod. Phys. Lett. B **8**, 535 (1994).
[19] G. Moeller, Q. Si, G. Kotliar, M. Rozenberg, and D. Fisher, Phys. Rev. Lett. **74**, 2082 (1995).
[20] G. Aeppli and Z. Fisk, Comments Condens. Matter. Phys. **16**, 155 (1992).
[21] M. J. Rozenberg, G. Kotliar, H. Kajueter, G. A. Thomas, D. H. Rapkine, J. M. Honig, and P. Metcalf, Phys. Rev. Lett. **75**, 105 (1995).
[22] M. Jarrell, H. Akhlaghpour, and Th. Pruschke, Phys. Rev. Lett. **70**, 1670 (1993); see also D. Hirashima and T. Mutou, Physica B **199**&**200**, 206 (1994).
[23] Th. Pruschke, D. L. Cox, and M. Jarrell, Europhys. Lett. **21**, 593 (1993).
[24] M. Jarrell, Phys. Rev. B **51**, 7429 (1995).
[25] M. Jarrell, J. K. Freericks, and Th. Pruschke, Phys. Rev. B **51**, 11 704 (1995).
[26] P. F. Maldague, Phys. Rev. B **16**, 2437 (1977).
[27] W. Kohn, Phys. Rev. **A 171**, 133 (1964).
[28] D. Baeriswyl, C. Gros, and T. M. Rice, Phys. Rev. B **35**, 8391 (1987).
[29] Anil Khurana, Phys. Rev. Lett. **64**, 1990 (1990).
[30] P. Coleman, Phys. Rev. B **29**, 3035 (1984); T. M. Rice and K. Ueda, *ibid.* **34**, 6420 (1986).
[31] M. J. Rozenberg, Phys. Rev. B **52**, 7369 (1995).
[32] C. Castellani, C. R. Natoli, and J. Ranninger, Phys. Rev. B **18**, 4945 (1978).
[33] L. F. Mattheiss, J. Phys. Condens. Matter **6**, 6477 (1994).
[34] J. H. Park, L. H. Tjeng, J. W Allen, P. Metcalf and C. T. Chen (unpublished).
[35] G. A. Thomas *et al.*, Phys. Rev. Lett. **73**, 1529 (1994).
[36] R. M. Moon, Phys. Rev. Lett. **25**, 527 (1970).
[37] S. Shin *et al.*, J. Phys. Soc. Jpn. **64**, 1230 (1995).
[38] D. Whittoff and E. Fradkin, Phys. Rev. Lett. **64**, 1835 (1990).
[39] D. Mc Whan *et al.*, Phys. Rev. Lett. **27**, 941 (1971); Phys. Rev. B **7**, 3079 (1973); S. A. Carter, T. F. Rosenbaum, P. Metcalf, J. M. Honig, and J. Spalek, *ibid.* **48**, 16 841 (1993).
[40] For details on the application the theory to models with long-range order, see Refs. 9, 16, and 31.
[41] J. Hubbard, Proc. R. Soc. London Ser. A **281**, 401 (1964).
[42] R. Preuss, W. Hanke, and W. von der Linden, Phys. Rev. Lett. **75**, 1344 (1995).
[43] A. Matsuura *et al.*, Phys. Rev. B **53**, R7584 (1996).
[44] A. Moreo, S. Haas, A. Sandvik, and E. Dagotto, Phys. Rev. B **51**, 12 095 (1995).
[45] L. Degiorgi *et al.*, Europhys. Lett. **28** 341 (1994).
[46] E. Gagliano *et al.*, Phys. Rev. **B 34**, 1677 (1986).
[47] Due to a conversion factor error, it was stated in Refs. 35 and 21 that the integrated spectral weight of V_2O_3 agreed well with the one band Hubbard Model. the inset corrects that of Ref. 21.